COMPUTER-AIDED DESIGN & APPLICATIONS, 2017
VOL. 14, NO. 4, 486–497
http://dx.doi.org/10.1080/16864360.2016.1257190

Software-aided measurement of geometrical fidelity for 3D printed objects

Felix W. Baumann, Jochen Wellekötter, Dieter Roller and Christian Bonten

University of Stuttgart, Gemany

ABSTRACT

This research evaluates the geometric fidelity of 3D printed objects by utilizing digital image analysis techniques on consumer grade 3D printers. ISO 527-2 Type B specimen are modeled using Houdini Software, then positioned on the virtual print-bed and sliced in 0.3 mm thickness layers utilizing MiracleGrue slicer. The specimens are printed on a Makerbot Replicator2X 3D printer with an X-Y resolution of 0.011 mm. The test set is divided into three where the first object set (Test set A) is printed with their longest side parallel to the X axis, the second object set (Test set B) with their longest side oriented at an angle to the X axis and the third object set (Test set C) as a control with a different material type and structure. The test includes objects with parallel patterns of 0, 5, 10, 30, 45, 60 and 90 degree resulting in toolpaths along the parallel lines. For the second test set the orientation angle is chosen to match the parallel pattern degree. The objects are analyzed with a software developed for this purpose. For image data acquisition a scanner is employed. This work shows that high quality geometric information can be deduced from scanned image data for the analysis of the geometric fidelity of flat or thin 3D printed objects. This work also displays enhancements possible to the proposed algorithm and software. With this research we present a low cost and unobtrusive method to perform geometrical analysis for flat printed additively manufactured objects. By providing a software component that is able to extract geometrical information from existing models (as STL or STEP files) and matches them digitally acquired images from printed objects we are able to ascertain the geometric fidelity of 3D printed objects under the influence of varying filling patterns and object orientation.

KEYWORDS

3D Print; Additive Manufacturing; Geometric Fidelity; Print Quality; Image Data

1. Introduction

Fused Layer Modeling (FLM, also Fused Deposition Modeling FDM or Fused Filament Fabrication FFF [7]) is a layer oriented Additive Manufacturing (AM) [11, 16, 19] technique that has evolved from Rapid Prototyping (RP), where a semi-molten thermoplastic, e.g., Acrylonitrile Butadiene Styrene (ABS), is extruded in strands through a heated nozzle of a print-head that is mobile in two directions (X-Y plane). In this article 3D printing is used interchangeable with AM and does not refer to the specific AM technology.

There is a variety of different 3D printing technologies enabling the use of various materials. 3D Printing technology is capable of processing metals with Electron Beam Melting (EBM) or Selective Laser Sintering (SLS) [8] and Selective Laser Melting (SLM), plastics as in the case of FDM (thermoplastics) or Stereolitography (SLA) (photopolymers) or sands and ceramics with sand casting or with 3D Printing (3DP) [7]. After completion of one layer the print-head or print-bed moves upwards or downwards, respectively, for the next layer to be worked upon. With FDM technology the material is fed to the extruder from a spool of plastic filament. The material is heated to about 230-250° Celsius (depending on material) in the extruder. This temperature is above the glass-transition temperature of ABS [3]. The extrudate is deposited on the print-bed or existing layers in a bead-wise fashion. When the material is heated and cooled down again its physical properties change and the material changes its specific volume (shrinkage) leading to defects in the geometry of the printed object in comparison to the original model [17].

This research is focused on consumer grade 3D printers and their capabilities to produce objects that match the original models closely. In order to clarify the focus on a specific class of machines the following classification is proposed.

FDM printers can be classified by precision or cost where professional 3D printers are expected to be more precise and faster than low-cost or consumer grade 3D printers. Consumer grade 3D printers [10] are oftentimes not equipped with a climate controlled closed build

CONTACT Felix W. Baumann baumann@informatik.uni-stuttgart.de

envelope in contrast to the industrial machinery. For the assessment of the capabilities to produce objects that match the original models, the geometric properties of the printed objects in an experiment are observed.

For this work the following two research questions are set:

1. Are consumer grade 3D printers capable of repeatedly producing objects that match the models within a certain dimensional tolerance?
2. How can the geometrical properties of printed objects be acquired with high repeatability and limited effort?

As a restriction on the models and objects processed we focus on flat (2 dimensional) objects.

Assessment of quality of 3D printed parts can be conducted by analyzing mechanical properties such as flexibility or strength, object properties such as roughness of surfaces, printability of various features such as holes of various diameters, overhangs of various angles, viable wall thickness or minimum diameter of protruding structures. The latter properties can be deducted printing special test models for 3D printers, which we did not use because of their inability to be scanned with a scanner and the need for further examination of strength and roughness properties. The end user is the most critical inspection instance in case of consumer grade printers and this instance is limited in the tools available for in-depth mechanical and or specialized analysis. Hence, the research on graphical or visual object inspection is justified.

In order to assess the quality of consumer grade 3D printer in respect to geometric fidelity and repeatability an experiment that requires limited human interaction and is therefore suitable for partial automation is devised. The assessment of the geometric fidelity is performed on specimen from the experiment utilizing a software developed for automated object analysis from scanned image data of specimen.

This experiment is conducted to ascertain the viability of extracting geometrical information from 3D printed objects via scanned images using software. The software utilization enhances the extraction quality of the geometrical information over manual measurements (i.e. using a caliper) and computer aided measurements (i.e. measuring dimensions of key-points in image manipulation software). As a secondary benefit of this experiment a compilation of high-quality scanned images of printed objects is created. This compilation poses an added benefit with the accompanying sensor output acquired during the manufacturing of the objects for post-mortem analysis. By experiment design we evaluate the geometric fidelity of 3D printed parts on consumer grade 3D printers in regard to the printing orientation and internal layer orientation.

2. Research contribution

In this section we describe the motivation for this experiment and the considerations for the implemented software. Following is a description of the experiment and the results from this experiment.

2.1. Motivation

For AM in general and FLM in particular there is often a mismatch between the model intended to produce and the resulting object printed. This is due a number of reasons for FLM printing [9]:

- Variations in the quality of filament (Low quality product or induced by product storage).
- Variations in the filament diameter and in the circularity of the filament.
- Motor slippage or incorrect positioning of the print-head.
- Material inherent changes due to the printing process (heating then cooling).
- Detachment of object due to warping or mechanical shock.
- Quality of 3D printer in positioning the print-head and print-bed.

This work is performed under the hypothesis that additionally to these factors, the geometry of the model influences the geometric fidelity of the printed object. With this research a method to evaluate the quality of a FLM 3D printer in respect to the geometric fidelity of the objects printed is proposed. This method is non-obtrusive, requiring no specialized hardware and is applicable after objects are printed.

2.2. Related work

This section reviews contemporary work that is related to geometric fidelity assessment and printing capabilities of the FLM and other printing processes. The works on geometric fidelity stem largely from the field of medicine and utilize bio printing.

The work of Cohen and Lipson [5] proposes a closed loop control system for droplet oriented solid freeform fabrication (SFF) which they name greedy geometric feedback (GGF). Within this work they analyze sources of geometric mismatches between the printed objects and the models. Their approach for resolving these problems

is a scanning technique for online instruction creation. Their approach is not directly applicable to consumer grade FLM technology as they base decisions on single droplet deposition and do not consider beadwise extrusion in their algorithm.

In a separate paper we describe the influence of various slicing tools on the perceived quality of the print [3]. For the analysis the surface quality of prints from different slicers the reproducibility of text and surface features is analyzed. Geometrical deviations were up to 57% (or 1.14 mm) for specific geometrical features. The slicers were found to have a great influence on the resulting quality of the object.

Hockaday et al. [12] also researched the shape fidelity of bio printed objects (porcine aortic valves). They conclude that 3D bio printed scaffolds can be fabricated with high geometric precision but that the accuracy decreases with smaller objects printed. They measured a geometric overlap (fidelity) between model and object ranging from 81.7% ± 1.9 to 61.9% ± 4.3 depending on the object size.

The work of Ballyns et al. [2] focuses on the shape fidelity of tissue-engineered objects with complex geometry. This work focuses on models printed with FLM technology and data acquired (reverse engineered) from MRI (Magnetic Resonance Imaging) and μCT (Micro Computer Tomography) machines. They measured a volumetric error of −21.7% ± 19.0 for prints from μCT data and −30.7% ± 9.4 for prints from MRI data. The repeatability error is 8.0% and 8.7% respectively.

In Duan et al. [6] the authors perform an experiment with 3D bioprinted alginate/gelatine substrate. Within this experiment they measure the printing accuracy to be within 84.3% ± 10.9 the models geometry. Their approach is for a biocompatible printing method that contains living cells on a substrate applied with a syringe.

Huang et al. [13] approach geometrical fidelity for additive manufacturing by altering CAD models before printing to account for expected deviations induced by the printing process. They apply their approach to cylindrical and polygonal shapes. Within their experiment on a SLA printer they measured the unaltered object deviation ranging from −0.006 to 0.02 inches depending on the objects geometry and size.

In the work of Ogden et al. [15] research is conducted into the influencing factors for geometrical accuracy of 3D printed objects on a Makerbot Replicator 2X using PLA. The focus of their work is the transformation of CT and MRI data to printable digital models and the influence of factors in the transformation process on the quality of the printed objects. In their experiment they found statistically relevant deviations in the print quality from the model, especially in the printers Z-dimension.

2.3. Methodology

The approach to this work is to extract geometrical information from high resolution scans of the object. Manual interaction for this requires the user to detach the object from the print-bed and place it onto a scanner. The software implementation extracts information on the length of the object and the widths at specified points from this image data. This process requires the object to be flat which is a limitation in the current implementation and the approach is only capable to determine geometric information in two dimensions. The specimens are of 0.3 mm height for this experiment.

The following processing flow for the extraction of geometrical information from CAD/STL model files and the physical printed objects is defined:

1. If model exists as STL then transform it to STEP
2. Extract model parameters from STEP files using FreeCAD and Python
3. Print model on 3D printer
4. Remove object from print-bed and attach to prepared paper form
5. Scan paper form in high resolution and lossless graphics format
6. Derive geometrical information from photographic scan using software

The geometrical information from the model and the object are stored in a database for comparison. This proposed method requires manual interaction from a user that removes the object and scans the paper form.

2.4. Implementation

All prints are executed with the same ABS filament on a Makerbot Replicator2X printer. The objects are left for cooling approximately 1 minute after the printing process finished. During the experimental prints sensor data on ambient and machine-inherent factors were gathered by a range of sensors in and attached to the 3D printer.

The software is based on the computer vision framework OpenCV (version 2.4.12.2) and implemented in Python (version 2.7.11). Geometrical information is extracted from both STL and STEP files of the model.

For the mid-section the edges from the STEP file within a defined range from the center (in the Y-axis) of the bounding box are analyzed and the average distance between them is calculated to determine the width of the middle part (inner width) of the object.

2.5. Experiment

All objects are printed using the parameters declared in the configuration file available in the Appendix (8.1). The models are generated so that the slicer can only follow the prescribed paths and cannot implement extrusion strategies of its own. The models are created to contain patterns [14] filling the surface with 0, 5, 10, 30, 45, 60 and 90 degrees orientation and are based on the EN ISO 527-2:1996 standard (Specimen 1B) with the alteration of the model thickness (Standard defines thickness h as 4.0 ±0.2 mm) to 0.3 mm. The thickness is chosen to only print one layer and research influences of the orientation on the stability. This research is to be published separately. See Fig. 3 for the values of the model dimensions. All models are of the same sizes and only differ in the orientation of the infill-pattern. See Fig. 2 for the design of the models and their pattern-orientation.

An experiment with 3 groups is devised, where group A contains objects printed with their longest side perpendicular to the X axis, group B objects are oriented with the longest side at an angle of α degrees against the X axis where α corresponds to the infill-angle of the pattern. Group C consists of objects printed in a different color as a test of the stability of the software. Objects from group C are also printed with two layers, i.e. these objects are double the height.

As the 3D printer cannot move diagonally but has to interpolate diagonal movement from X and Y movement, overlay objects from group A (with the exception of special case of 0 degree pattern orientation) have shorter movement paths with only one axis involved. The objects are printed in ABS (ABS 1.75 mm Pink Lion&Fox, Hamburg, Germany and ABS 1.75 mm Yellow, REC, Moscow, Russia). The color of the filament was selected to be purple and yellow (see Fig. 1) for verification that the software is capable of detecting object geometry independent of object color.

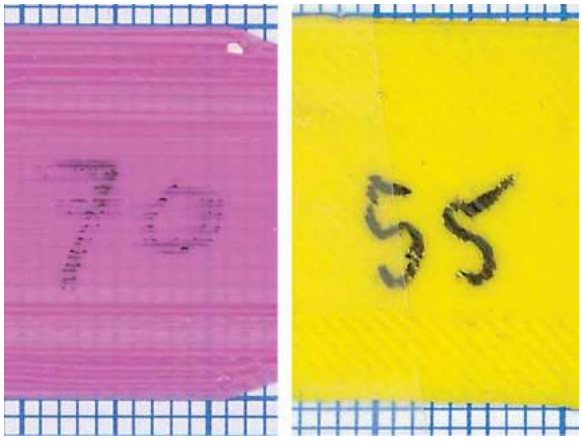

Figure 1. Colors used for experiment. Purple (left) and yellow (right).

For this experiment the following hypotheses are formulated:

1. The more straight lines (only involving one motor/axis) the toolpath contains the more accurate the fabricated object is to the model.
2. The geometric fidelity of a consumer grade 3D printer for simple geometries is accurate to within 5 percent of the objects dimension.
3. The automated geometrical analysis of (flat) printed objects is possible utilizing a scanner. The error in measurement is less than 2 percent.

The forms with the attached objects are scanned using a Konica Minolta bizhub 42 integrated office printer-scanner at a resolution of 600×600 dpi (Dots per Inch). This resolution leads to a theoretical pixel count per centimeter of 236.22047.

$$1\text{cm}^{-1} = \sqrt{\frac{600^2}{2.54^2}} \tag{1}$$

This theoretical pixel to centimeter count corresponds well with manually measured values for horizontal resolution of 235.556 pixel/cm (99.7% of theoretical value) and 235.91 pixel/cm (99.87% of theoretical value) for vertical resolution. These values are averaged over all manual measurements.

2.6. Experiment results

A total of 135 objects are analyzed using the software and manual measurement. Group A consists of 64 elements, group B of 26 elements and group C of 57 elements. Objects from the special case of zero degree pattern are counted for group A and group B. From group C 12 objects are discarded as their prints failed for the reason of communication errors. To verify the accuracy of the system all objects are measured manually utilizing graphical measurements.

See Fig. 4 for details on the movement types that occur within each object. In Tab. 1 the absolute number of movements per type is listed with the table header abbreviations of # Moves for the total number of movement instructions within the file, # No-Move for the total number of instructions that do not move the print-head, e.g., retraction instructions, #X-Only and #Y-Only for instructions that only move the print-head in X or Y direction but not the other, #X-Dominant and #Y-Dominant for instructions that move the print-head in both axes but either X or Y axis is dominant and # X-Y

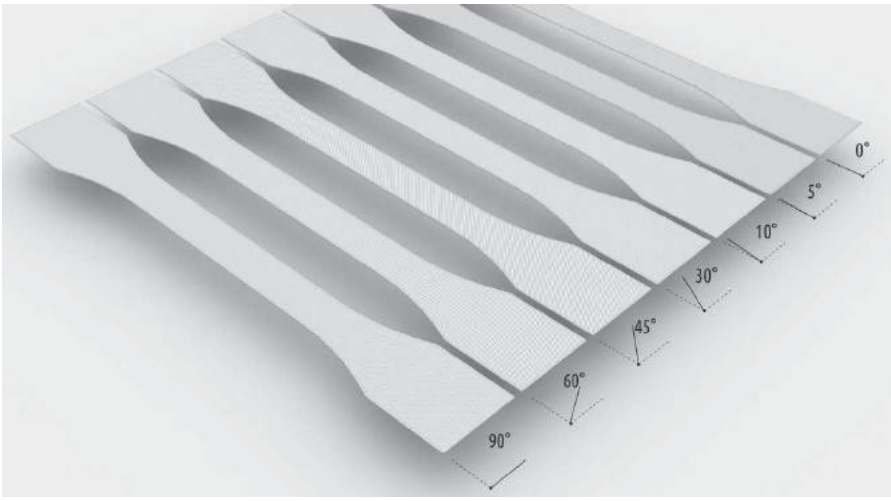

Figure 2. Pattern orientation for specimen.

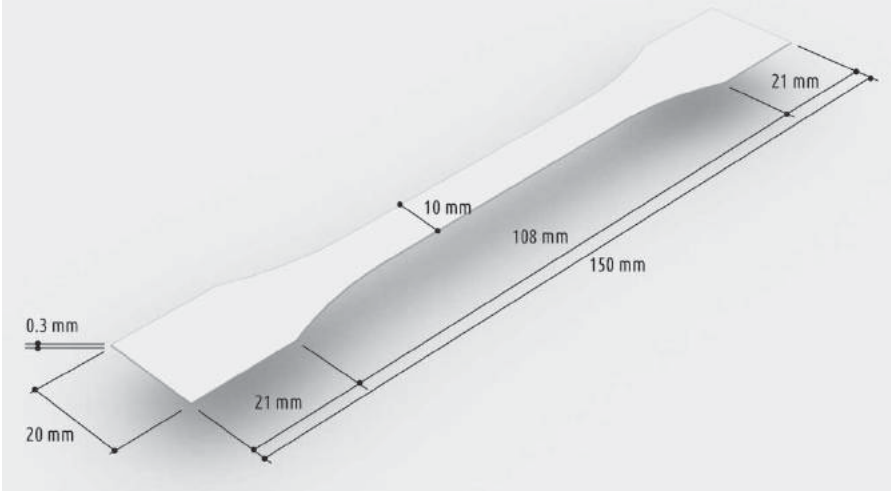

Figure 3. Geometric properties of specimen.

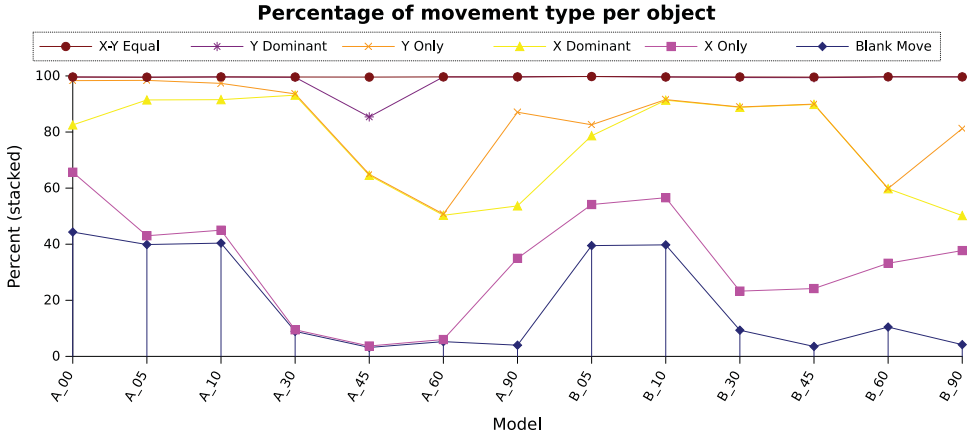

Figure 4. Percentage of movement type per model.

Table 1. Movement information per model.

Model	# Moves	# No-Move	# X-Only	# Y-Only	# X-Dominant	# Y-Dominant	# X-Y Equal
A 0	848	376	181	134	143	11	0
A 5	702	280	22	49	340	8	0
A 10	911	368	42	53	424	21	0
A 30	863	77	5	4	722	51	1
A 45	782	25	4	3	476	160	111
A 60	930	49	7	4	412	455	0
A 90	952	38	295	318	178	120	0
B 5	1529	604	224	60	375	263	0
B 10	880	350	148	2	306	71	0
B 30	868	81	121	1	569	92	1
B 45	789	28	163	1	518	74	2
B 60	1042	109	237	1	277	415	0
B 90	954	40	320	296	119	176	0

Equal for instructions that move the print-head by the same amount in X and Y, i.e. diagonal movement.

For the length of the specimen the systematic error (predictable, due to, e.g., shrinkage) due to shrinkage appears dominant as the standard deviations for all group are smaller (See Fig. 7) and with the exception of the 5, 10 and 90 degrees specimen all specimen from set B are within a 2% tolerance of the expected value. From the standard deviation and the grouping of the specimen it appears that random printing errors have less influence on this dimensional measurement. For the width measurements the error margins increase for set A and B up to 45 degrees and then decrease again (See Fig. 5). Only objects with 45 degree infill pattern printed at 45 degrees (Set B) are within the expected ±2% tolerance of the width measurements. For inner width measurement the plotted percentiles (See Fig. 6) and data indicate a high influence of random errors. Only objects printed with a 5 degree infill pattern printed at 5 degree orientation (Set B) are located within the 2% tolerance margin.

2.6.1. Measurement results per model

In this section we describe the results measured throughout the experiment. In Figures 5ff the measured values for the respective dimension is shown under separation for each pattern and orientation (Test group A is abbreviated with "hor" and Test group B is abbreviated with "oriented"). Furthermore the aggregated values for the respective dimension are displayed (All) and the aggregated values for test group A (All (hor)) and test group B (All (oriented)). Dashed lines in the figures indicate the expected values and margins according to EN ISO 527:2-1996.

Within group A (horizontally aligned) the following measurements are taken. For the length of the printed objects the average measured value was 14.78 cm, the median value was 14.79 cm and the standard deviation 0.124 cm. The width of the object averaged at 2.01 cm with a median of 2.00 cm and a standard deviation of 0.024 cm. The inner width averages at 1.04 cm with a median of 1.04 cm and a standard deviation of 0.028 cm.

For group B (orientation with the pattern direction) the following measurements are taken. For the length of the printed objects the average measured value was 14.73 cm, the median value was 14.82 cm and the standard deviation 0.129 cm. The width of the object averaged at 2.01 cm with a median of 2.02 cm and a standard deviation of 0.027 cm. The inner width averages at 1.04 cm with a median of 1.04 cm and a standard deviation of 0.037 cm.

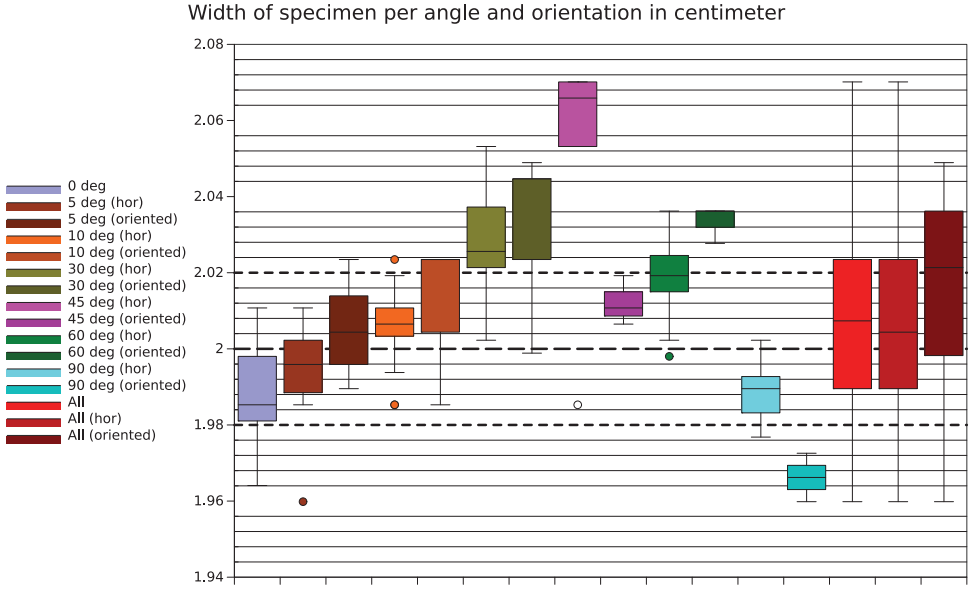

Figure 5. Length of specimen per angle and orientation (in centimeter).

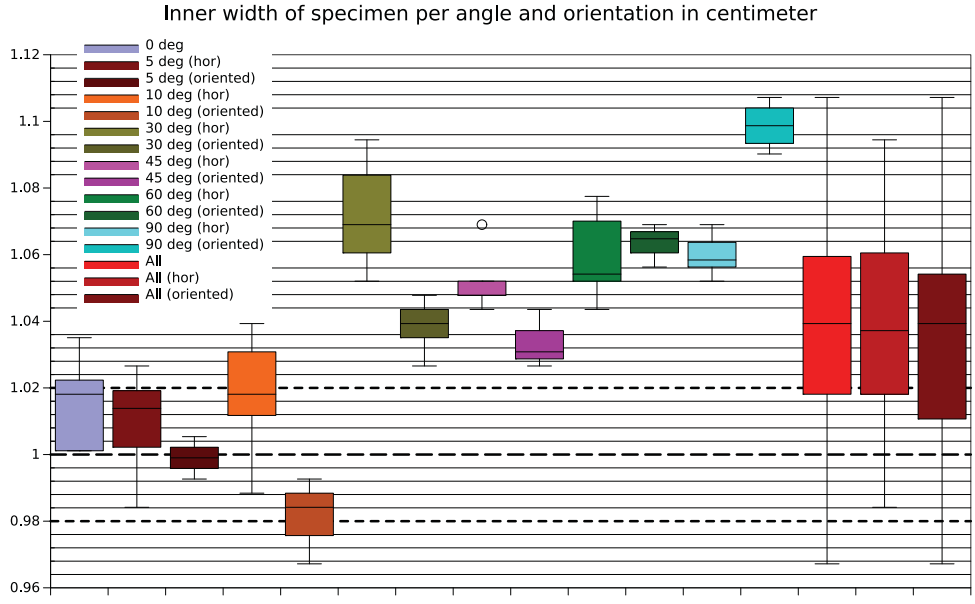

Figure 6. Inner width of specimen per angle and orientation (in centimeter).

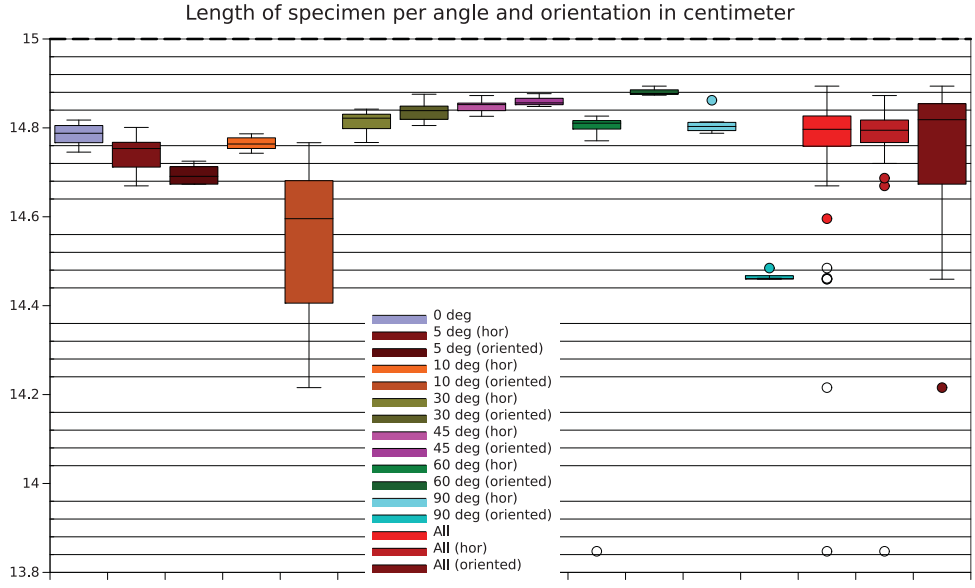

Figure 7. Length of specimen per angle and orientation (in centimeter).

For group C (dual layer, yellow color) the following measurements are taken. For the length of the printed objects the average measured value was 14.67 cm, the median value was 14.82 cm and the standard deviation 0.045 cm. The width of the object averaged at 1.99 cm with a median of 2.01 cm and a standard deviation of 0.018 cm. The inner width averages at 1.06 cm with a median of 1.05 cm and a standard deviation of 0.021 cm. In Fig. 8 a tighter grouping of the measured values for group C is displayed. The expected value for the respective dimension is indicated by a dashed green horizontal line and the 5% margins are indicated by solid red horizontal lines. The boxplots in Fig. 8 display the median value for each measurement group, the first (lower box line) and third percentile (upper box line), the minimum and maximum (lower and upper whisker) and outliers indicated by circles.

Overall measurements combined the length is on average 14.76 cm, with a median of 14.8 cm and a standard deviation of 0.143 cm. The average combined width is 2.00 cm, with a median of 2.00 cm and a standard deviation of 0.025 cm. The inner width averages at 1.04 cm

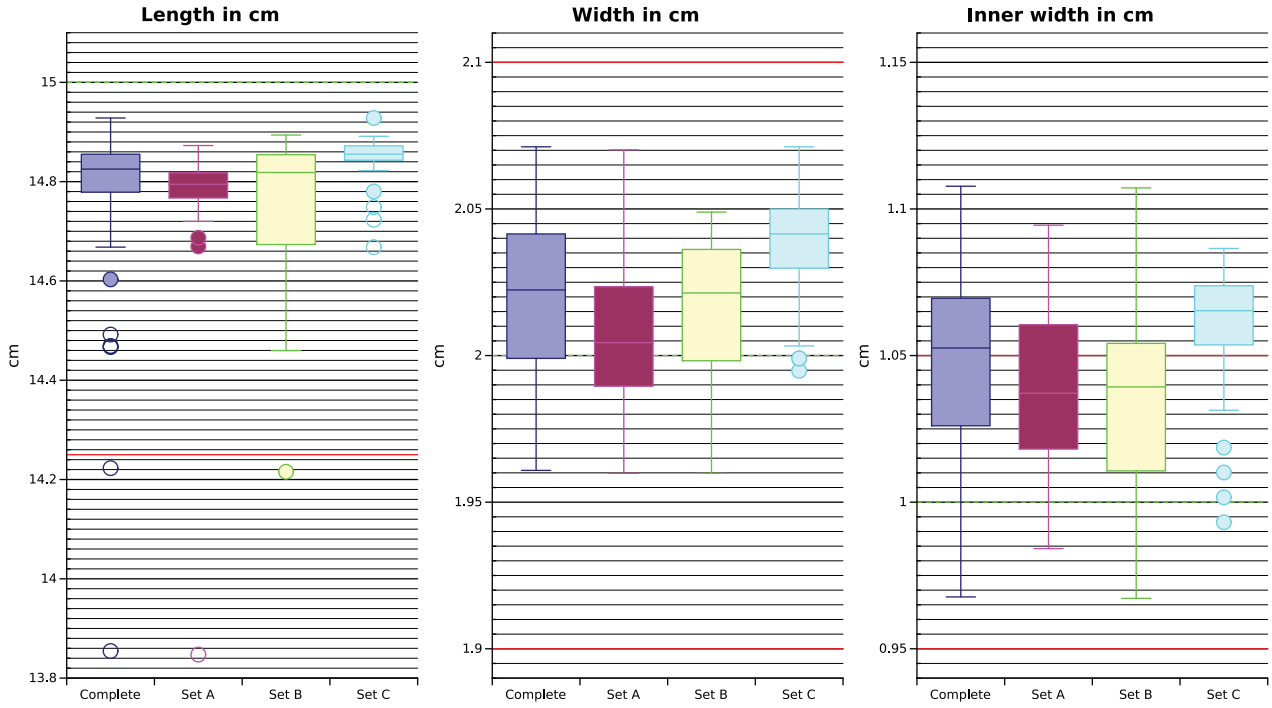

Figure 8. Measurement of dimensions for specimen. Length in centimeter (left), inner width in centimeter (middle) and width in centimeter (right).

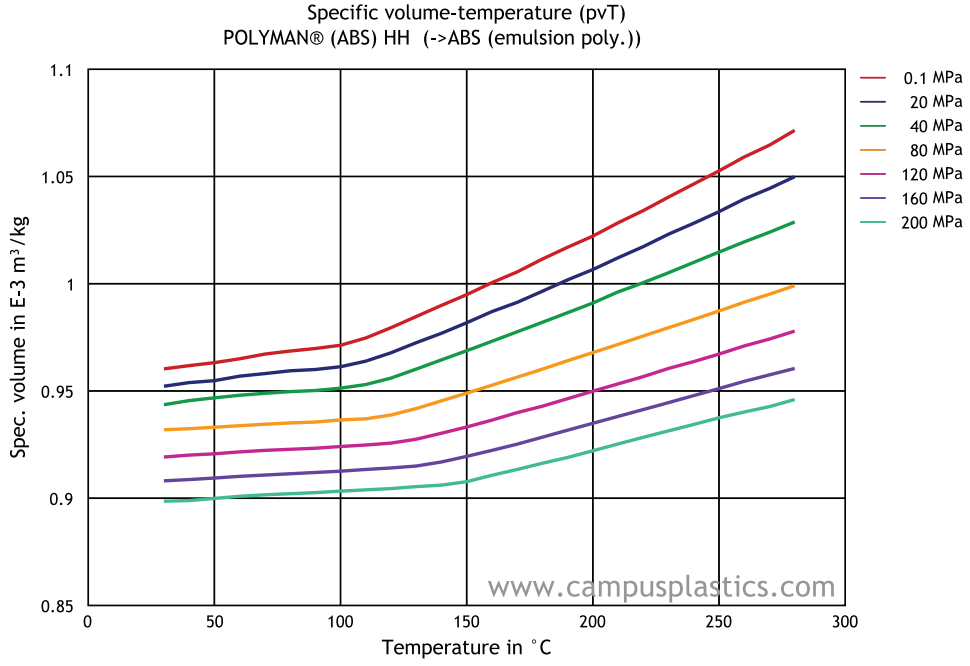

Figure 9. pvT diagram for ABS,

with a median of 1.04 cm and a standard deviation of 0.03 cm.

A certain amount of volume shrinkage of ABS during processing is expected. Fig. 9 shows a specific volume-temperature (pvT) diagram for POLYMAN® (ABS) from A. Schulman Inc, Fairlawn, Ohio [1]. Given a processing temperature of 250 °C, we find a specific volume of ABS of approximately 1.05 E^{-3} m^3/kg. At room temperature the specific volume is 0.96 E^{-3} m^3/kg, which results in a shrinkage of 9% [15, 16].

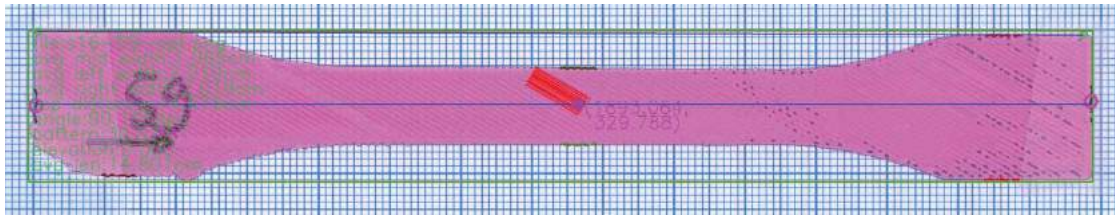

Figure 10. Specimen 59 as read by the software (scanned data).

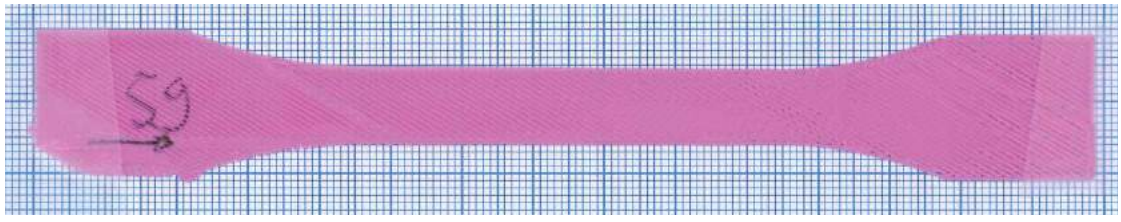

Figure 11. Annotated specimen 59 after analysis by software.

2.6.2. Results for software extracted geometry

From the overall set of available object scans a subset of 50 was chosen to measure the objects geometry. The software failed in 10 cases due to mis-detected object boundaries. The remaining 40 measurements are in accordance with the manually measured dimensions. For the length measurement the average measured length difference is 9.366 pixel (2.25%), the median is −4.699 pixel (−0.047%). The measurement difference for the width at the right side is on average −58.503 pixel (−15.15%) and the median is −14.4 pixel (−3.23%). For the left side width the measurement difference is on average 5.88 pixel (−1.3%) and the median −6 pixel (−1.38%). For the central width the measurement difference is on average 8.38 pixel (1.1%) and the median is −3 pixel (−1.26%). The fact that the right side is mis-printed (e.g., fanned out, missing or bent) in some models can explain the measurement discrepancies for the width at the right hand side.

In Fig. 10 the specimen number 59 is shown as the software reads the image data. It is segmented from a form that contains a multitude of objects (form format is A4). It is scanned against a background that has a millimeter mesh printed on. In Fig. 11 the resulting output of the software is displayed as an example. The green boundary around the object is the bounding box around the identified blob. In the middle there is a purple dot with coordinates indicating the detected center of gravity from which the measurements for the inner width are conducted (indicated by wiggly lines above and below center point). The red lines at the center of gravity are visualization aids for determining the objects pattern. Information is overlaid on the left border of the object for easier human interaction. The line through the center (blue) indicates the measured length from averaged points at the left and right hand side of the object.

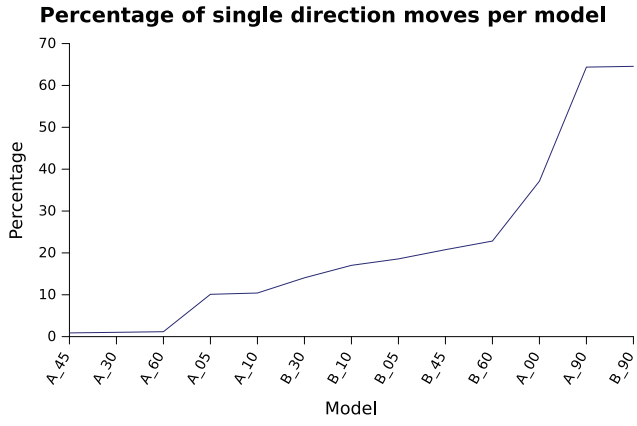

Figure 12. Percentage of single direction moves per model.

3. Evaluation/discussion

For the hypotheses set before:

1. The more straight lines (instructions only involving one motor/axis) the toolpath contains the more accurate the fabricated object is to the model.
2. The geometric fidelity of a consumer grade 3D printer for simple geometries is accurate to within 5 percent of the objects dimension.
3. The automated geometrical analysis of (flat) printed objects is possible utilizing a scanner. The error in measurement is less than 2 percent.

We can conclude that:

1. In Fig. 13 the root mean square error (RMSE) per model and measurement dimension is plotted. The RMSE for the length dimension (green line) has the largest influence on the averaged RMSE per model (dashed light blue line). The test sets for B 10, A 60 and B 90 have a visibly larger RMSE than the other test sets but only model B 90 can be identified with a very high percentage of single axis movement instructions. This hypothesis cannot be verified. Fig. 12 provides information (see also Tab. 1) on the aggregated percentage of single dimensional move instructions for each model. Information on the movement is directly extracted from the machine code.
2. This is true for averaged results of length and width of the objects. Individual results vary for more than 5 percent of the intended geometry. For the inner width this hypothesis does not hold true as the median inner width is greater than 5 percent of the model parameter (5.3%). The length of objects from group B with a 10 degree pattern varied the most in their measured dimensions. The absolute error for the width and inner width measurements is smaller than for the measurement of the length as it can be seen in the graph for the mean square error per dimension (see. Fig. 12). As the 3D printer cannot scale its accuracy in response to the models structure but only position the print-head and print-bed based on the accuracy of the motors, motor controls and associated parts this behavior expected and

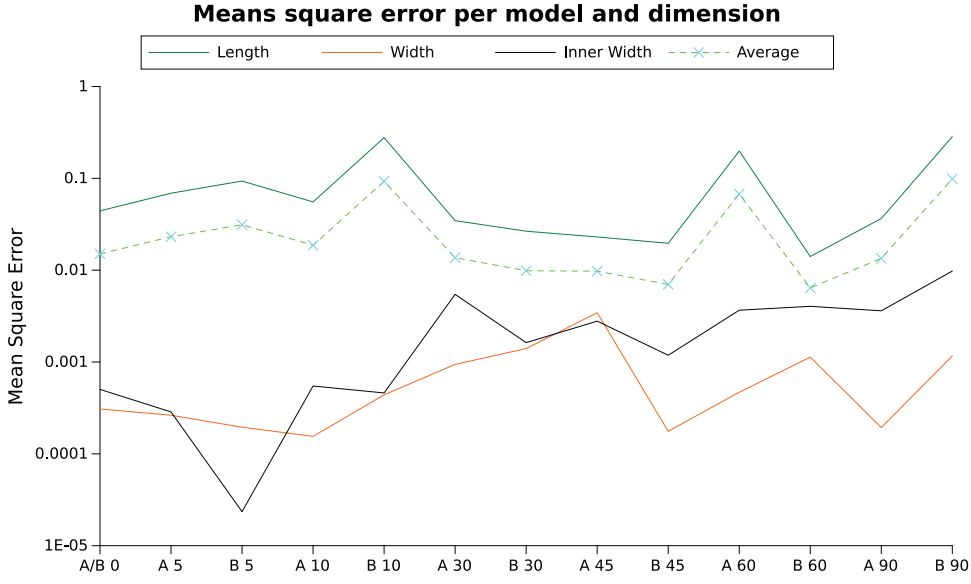

Figure 13. Mean square error per model and dimension (log-scale).

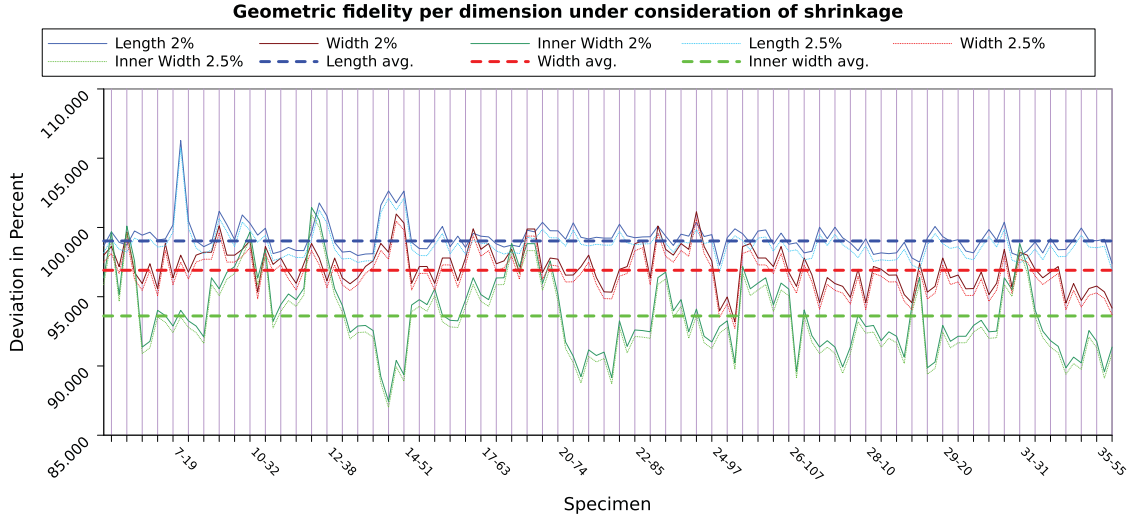

Figure 14. Geometric fidelity per dimension under consideration of shrinkage.

valid. One explanation for the fact that the RMSE for the length measurement is about 2–3 orders of magnitude larger than the remaining measurements can be the effect of shrinkage while cooling. For an assumed shrinkage of 1% per 100°C any dimension will be 2-2.5% shorter than the model for an extrusion temperature of 245° C and a room temperature of 25° C. For the original dimensions of length, width and inner width this will result in measured dimensions of:

- Length: 14.625–14.7 cm
- Width: 1.9–1.96 cm
- Inner width: 0.975–0.98 cm

When taking this shrinkage into consideration the measurements per dimension all lay on average within 93.61% of the expected range. See Fig. 14 for a plot of all shrinkage adjusted measurements per dimension (Length in blue, width in red and inner width in green) with the average fidelity as thick dashed lines in the respective colors. The average adjusted fidelity for the length dimension is 99.03%, for the width dimension it is 96.91% and for the inner width dimension it is 93.61%. In Fig. 14 the labeling for the X-axis is the original object identifier used for the experiment and no indication to group or model given. The above graph is to visualize the average adjusted geometric fidelity per measurement dimension. The variations are largest for the inner width dimension as the tolerances are smallest here. The standard deviation measured is 1.119%, 1.496%, 2.775% for the length, width and inner width at an expected 2% shrinkage and 1.113%, 1.488% and 2.760% for 2.5% shrinkage respectively.

3. This is true with the exception of mis-printed parts that are to be identified manually before processing as the detection capabilities are insufficient. The identification of the objects needs stabilization and failed models must not be attempted to scan with the software. As an improvement on the detection of the object we use blank white paper without any markings. This can avoid mis-detected object parts thus improve detection quality. Furthermore, with this research a baseline for this scanner is established and conversion factors from pixels to centimeters for this setup are present. Changes in any component of the workflow require a re-establishment of the baseline.

4. Summary

With this work we show that it is possible to utilize commercially available scanners to capture image data of the geometry of printed objects and to use software to extract from this image data geometrical information of the objects. We verify that the implemented software is capable of acquiring the object geometry with an error of the median value of less than 5 percent for flat objects independent of the objects color. Consumer grade 3D printers are capable of printing objects that differ in less than 5 percent of the model for larger (more than 1 cm) structures.

5. Outlook

For future research we develop of a system that captures the shrinking process during cooling of a printed object. Such a system can be based on video capture in order to precisely capture the cooling process and to better understand the influence of geometry on the geometrical deviations between model and object. This system can also be used to detect build failures or deviations from the model during printing enabling a timely response thus reducing waste material and time from mis-prints. Furthermore, we propose to extend this approach to true 3 dimensional objects with image data acquisition by high resolution cameras and the transform of the captured image data to 3 dimensional models for conformance checks against the model.

Acknowledgments

We would like to thank David Correa for his help with this work by designing the objects.

Due to size considerations results, raw data and scalable vector graphics of figures are available at http://doi.org/10.5281/zenodo.159676.

ORCID

Felix W. Baumann http://orcid.org/0000-0001-5292-3040
Jochen Wellekötter http://orcid.org/0000-0003-4232-2131
Dieter Roller http://orcid.org/0000-0002-2438-5676

References

[1] A. Schuhmann Inc.: POLYMAN® (ABS) data sheet
[2] Ballyns, J. J.; Cohen, D. L.; Malone, E.; Maher, S. A.; Potter, H. G.; Wright, T.; Lipson, H.; Bonassar, L. J.: An Optical Method for Evaluation of Geometric Fidelity for Anatomically Shaped Tissue-Engineered Constructs, Tissue Engineering Part C: Methods, 16(4), 2009, 693–703. http://dx.doi.org/10.1089/ten.tec.2009.0441
[3] Baumann, F.; Bugdayci, H.; Grunert, J.; Keller, F.; Roller, D.: Influence of slicing tools on quality of 3D printed parts, Computer-Aided Design and Applications, 13(1), 2016, 14–31. http://dx.doi.org/10.1080/16864360.2015.1059184
[4] Bonten, C.: Kunststofftechnik, Einführung und Grundlagen. Hanser, München 2014 – ISBN 978-3-446-440 93-7

[5] Cohen, D. L.; Lipson, H.: Geometric feedback control of discrete-deposition SFF systems, Rapid Prototyping Journal, 16(5), 2010, 377–393. http://dx.doi.org/10.1108/13552541011065777

[6] Duan, B.; Hockaday, L. A.; Kang, K. H.; Butcher, J. T.: 3D Bioprinting of heterogeneous aortic valve conduits with alginate/gelatin hydrogels, Journal of Biomedical Materials Research Part A, 101A(5), 2013, 1255–1264. http://dx.doi.org/10.1002/jbm.a.34420

[7] Gebhardt, A.: Generative Fertigungsverfahren. Hanser, München 2013 – ISBN 978-3-446-43651-0

[8] Gibson, I.; Shi, D.: Material properties and fabrication parameters in selective laser sintering process, Rapid Prototyping Journal, 3(4), 1997, 129–136. http://dx.doi.org/10.1108/13552549710191836

[9] Goebel, L.; Bonten, C.: More biobased plastics for 3D-Printing. European Bioplastics Conference, 2014

[10] Gribbins, C.; Steinhauer, H. M.: Experimental analysis on an additively manufactured abs living hinge. Solid Freeform Fabrication (SFF) Symposium, 1212–1224, 2014, 010

[11] Guo, N.; Ming, C.; Leu, M. C.: Additive manufacturing: technology, applications and research needs, Frontiers of Mechanical Engineering, 8(3), 2013, 215–243. http://dx.doi.org/10.1007/s11465-013-0248-8

[12] Hockaday, L. A.; Kang, K. H.; Colangelo, N. W.; Cheung, P. Y. C.; Duan, B.; Malone, E.; Wu, J.; Girardi, L. N.; Bonassar, L. J.; Lipson, H.; Chu, C. C.; Butcher, J. T.: Rapid 3D printing of anatomically accurate and mechanically heterogeneous aortic valve hydrogel scaffolds, Biofabrication, 4(3), 2012, 00–01. http://dx.doi.org/10.1088/1758-5082/4/3/035005

[13] Huang, Q.; Nouri, H.; Xu, K. ; Chen, Y.; Sosina, S.; Dasgupta, T.: Predictive modeling of geometric deviations of 3D printed products - A unified modeling approach for cylindrical and polygon shapes, Automation Science and Engineering (CASE), 2014 IEEE International Conference on, 25–30, 2014, http://dx.doi.org/10.1109/CoASE.2014.6899299

[14] Kanada, J.: Method of designing, partitioning, and printing 3d objects with specified printing direction. Proceedings of ISFA2014, 2014, http://ykanada.sakura.ne.jp/3dprint/NatDir3DP-ISFA14.pdf

[15] Ogden, K. M.; Aslan, C.; Ordway, N.; Diallo, D.; Tillapaugh-Fay, G.; Soman, P.: Factors Affecting Dimensional Accuracy of 3-D Printed Anatomical Structures Derived from CT Data, Journal of Digital Imaging, 28(6), 2015, 654–663. http://dx.doi.org/10.1007/s10278-015-9803-7

[16] Pham, D. T.; Gault, R. S.: A comparison of rapid prototyping technologies, International Journal of Machine Tools and Manufacture, 38(10–11), 1998, 1257–1287. http://dx.doi.org/10.1016/S0890-6955(97)00137-5

[17] Stava, O.; Vanek, J.; Benes, B.; Carr, N.; Měch, R.: Stress Relief: Improving Structural Strength of 3D Printable Objects, ACM Trans. Graph., 31(4), 2012, 48:1–48:11. http://doi.acm.org/10.1145/2185520.2185544

[18] Wang, X.: Calibration of shrinkage and beam offset in SLS process, Rapid Prototyping Journal, 5(3), 1999, 129–133. http://dx.doi.org/10.1108/13552549910278955

[19] Wong, K. V.; Hernandez, A.: A Review of Additive Manufacturing, ISRN Mechanical Engineering, 2012. http://dx.doi.org/10.5402/2012/208760